A Failure Criterion of Weak and Crushable Limestone Rock in Mining Field containing Karstic Cavities

Yahya Alassaf
Civil Engineering Department, College of Engineering, Northern Border University, Saudi Arabia
alassafy@gmail.com

Abdelkader Mabrouk
Civil Engineering Department, College of Engineering, Northern Border University, Saudi Arabia
abdjih2019@gmail.com (corresponding author)

Mehrez Jamei
Civil Engineering Department, College of Engineering, Northern Border University, Saudi Arabia
mehjamei@yahoo.fr

Anwar Ahmed
Civil Engineering Department, College of Engineering, Northern Border University, Saudi Arabia
Anwar.ahmed@nbu.edu.sa

Received: 19 March 2024 | Revised: 14 April 2024 | Accepted: 14 April 2024

 DOI: https://doi.org/10.48084/etasr.7295

ABSTRACT

This study aims to correlate the mechanical properties measured in the laboratory and the field for weak and crushable limestone in a mining site containing random karstic cavities. Compressive tests were performed in the laboratory to obtain Unconfined Compressive Strength (*UCS*) and rock mass modulus (E_{rm}). Field tests were: i) boring and drilling cores that allowed obtaining Rock Quantification Distribution (*RQD*) and recovery rock parameter (*REC*), and ii) Ground Penetration Radar (GPR) to detect and locate random cavities in the underground limestone deposit. The correlation between the E_m/UCS rate and the *RQD* was determined and analyzed. Based on the role of the new interpretation of the Geological Strength Index (GSI) and its relationship with the E_{rm}/UCS rate, a mathematical relationship was determined to link *GSI* and *RQD*. This relationship was a basis for modifying the generalized Hoek-Brown criterion, involving the amplitude of reflected electromagnetic waves (EM) provided by GPR field tests.

Keywords-weak limestone rock; Unconfined Compressive Strength (UCS); rock mass modulus (E_m); Rock Quality Designation (RQD); Karstic cavities; Ground Penetration Radar (GPR)

I. INTRODUCTION

The behavior of rock masses has been widely investigated, and laboratory results are generally associated with field observations. The conjunction between the two sources of data characterizes the majority of constitutive laws and the failure criterion by evaluating the corresponding parameters. By combining geological observations with laboratory test results, engineers and geologists can develop a comprehensive understanding of the behavior of rocks and predict their response to different stress and environmental factors. This knowledge is crucial for designing safe and sustainable engineering projects, namely tunnels, dams, slopes, and foundations, that rely on the stability and performance of rock materials [1-4]. Weak rock mass behavior refers to the mechanical response of rocks that have lower strength and stability compared to intact rock formations. This can occur due to factors, such as geological discontinuities, weathering, or structural weaknesses within the rock mass. Understanding the behavior of weak rock masses is crucial in various engineering and construction projects, as it can affect the stability and safety of infrastructure, like tunnels, slopes, and foundations. By studying the behavior of weak rock masses, engineers can develop effective strategies to mitigate potential risks and ensure the long-term durability of structures built on or within these formations. A literature review manifested that there are few correlation studies between field and laboratory test results, particularly for weak rocks.

In [3], a rock weathering classification system was proposed based on engineering properties, involving load index ($Is_{(50)}$), slake durability index (I_{d2}), density, mineralogy, and microstructure. Associations between parameters were used to develop engineering classification systems that provide an estimate of the engineering properties of weathered rocks. On the other hand, many empirical relations have been proposed for compressive strength (UCS) and stiffness. Other statistical connections have been proposed, but only between mechanical parameters measured in the laboratory [2]. Correlations between field and laboratory data are rarely proposed. Furthermore, field tests, such as in situ testing methods like borehole logging, pressuremeter tests, and geophysical surveys (seismic and ground penetration radars) provide valuable information about the geotechnical properties and conditions of the rock mass in its natural state. These tests can help identify geological features, discontinuities, and weaknesses that may affect the overall stability and behavior of the rock [5-8]. Ground Penetration Radar (GPR) offers several advantages compared to other field tests, as it can indirectly detect hidden faults and embedded elements without causing any destruction. For example, it enables the location and identification of cavities [9-12]. Furthermore, the common failure criterion for brittle and weak rocks is the Hoeke-Brown criterion [13-14]. The 2018 edition of the criterion was proposed to incorporate all modifications based on the experiences gained in applying it to practical problems [15]. Although the properties of fractured rocks considering the orientation and spacing of discontinuities have been relatively studied [16-18], the behavior of weak rocks, particularly crushable rocks, requires further investigation [19, 20].

This study investigates weak and crushable limestone in a mining site where civil engineering works have been planned. The new proposed idea is to combine geotechnical methods in the laboratory and field and GPR tests. This study begins by presenting the compressive test results of UCS and the rock mass modulus (E_m) and then conects the E_m/UCS rate to the Rock Quantification Distribution (*RQD*). The results in [15] are used to define the correlations between E_m/UCS and the geological index (*GSI*), and a mathematical relationship was obtained for weak and crushable limestone. As a result of the correlations and mathematical relationships, *GSI* was defined as a function of *RQD* for the limestone studied. Furthermore, based on a near-surface GPR survey, the karstic cavities were localized by interpreting the parabolic reflected waves and their amplitudes (A_i). A new change of the *GSI* parameter in the widely used generalized Hoeke-Brown criterion was proposed for a mathematical relationship between *GSI*, *RQD*, and the A_i/A_0 rate, where A_0 is the reference wave's amplitude.

This study presents some novelties that focus on three main aspects. The study concerns the behavior of the high crushable limestone. To the authors' knowledge, such rocks have previously been studied only a little. Adding to that, this study aims to relate GPR and geotechnical data, focused on the RQD collected from field experiences. To reduce the effect of the stochastic variability of RQD, some deterministic relationships were established to relate compressive resistance (UCS) to stochastic data (RQD). The third novelty is to consider the presence of cavities across the GPR information, characterized by the shape and the amplitude of magnetic waves. New mathematical relationships are proposed to link *RQD*, dimensionless waves' amplitude (A_i/A_0), and the commonly deployed *GSI* index. *GSI* is a field index that is often utilized in geologist recommendations. Some previous studies focused on the establishment of relationships between *RQD* and *GSI*. A modification of the mathematical expression of the Hoeke-Brown criterion is proposed that includes the relation between *RQD* and *GSI* and the instantaneous amplitude of EM waves.

II. LABORATORY TESTS AND FIELD INVESTIGATION

A. Laboratory Results of the Limestone Rock Deposit

Laboratory tests were performed to characterize the soil, including sieve analysis, Atterberg limits, and physical (dry density, water content) and unconfined compression tests. The findings showed that the soil consists of limestone rock with crystalline calcite. Figure 1 shows a typical GSD of the crushable part of the limestone rock. The area from which the samples were provided was (712×665 m). GSD was obtained for several specimens, as shown in Table I. Sieve analysis indicated that a huge part of the broken part of the cored specimens (obtained by drilling) corresponds to crushable limestone and gives a grain of an equivalent diameter between 7 cm and 2 mm. Crushable limestone is a typical behavior of weak limestone and expects the possibility of transition of rock to soil even by static mechanical loading. This is a real issue for the stability of the foundation, which should be compromised by an important elastic settlement. In addition, the friction resistance mobilized at the interface between the foundation (the case for piles) could be influenced by the crushing and it is significantly reduced. Using the ASTM classification, it can be concluded that the soil is sand mixed with on average 15% gravel and 15% fine soil (silt and clay). This is a wrong conclusion when examining the liquid and plastic limits that are not possible to measure (the fine amount of soil corresponds to the amount of highly crushable limestone). Table I summarizes the results and shows the homogeneous formation of crushable limestone by drilling, where the equivalent diameter ranges mainly between 0.075 mm and 7 cm. The formation percentage of the crushable quantity ranges between 65 and 70% (diameter equivalent to sand diameter range). The water content measured for the samples at depths of 0.5 to 10 m was relatively low, falling within the range of 1.5 to 2.5%. Table II shows UCS and E_m measurements.

TABLE I. PERCENTAGE OF CRUSHABLE PART OF THE LIMESTONE

Sample	% Gravel	% Sand	% Fine soil
B-2-1	17.8	68.2	14
B-6-1	19.5	65.2	15.3
B-9-1	20.1	66.5	13.4
B-12-2	22.9	62.1	15
B-12-4	15.3	70.9	13.8
B-16-1	18.9	65.8	15.3
B-20-3	19.2	66.6	14.2
B-24-2	16.7	69.8	13.5
B-27-4	19.2	67.1	13.7
B-30-3	15.9	69.1	15

TABLE II. PHYSICAL AND MECHANICAL PROPERTIES OF THE MASS ROCK MEASURED IN THE LAB

Specific gravity (*Gs*)	Measured unconfined compression strength (σ_c, MPa)	Average rock mass modulus (E_m, MPa)
2.633	8.16	1.94
2.619	8.31	2.77
2.622	8.89	2..10
2.626	8.09	1.93
2.621	12.75	3.93
2.582	12.75	2.45
2.623	13.82	2.50
2.623	16.18	2.85
2.612	14.48	3.25
2.585	15.76	3.50

An empirical relationship between *UCS* and E_m was derived from the experimental results (1). The results of compressive strength and stiffness indicate the weak state of the limestone and its highly weathered character (well-crushable).

$$Em = 0.52\left(\frac{UCS}{1+\sqrt{UCS}}\right) \quad (1)$$

III. GEOTECHNICAL FIELD TESTS

The *RQD*, defined by (2), was determined by drilling a large number of cored specimens. The recovery rock parameter (*REC*), defined by (3), was also determined. Figure 1 shows a regression between the two parameters.

$$RQD = \frac{\sum_1^n length\ of\ pieces,\ more\ or\ equal\ to\ 10cm}{Total\ Length\ of\ the\ drilled\ sample}(\%) \quad (2)$$

$$REC = \frac{\sum_1^n length\ of\ pieces\ obtained\ by\ boring}{Total\ Length\ of\ the\ drilled\ sample}(\%) \quad (3)$$

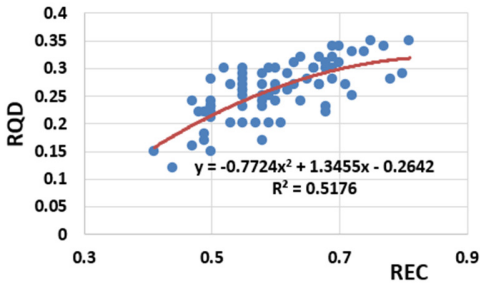

Fig. 1. RQD as a function of REC (results obtained by drilling in the investigated mining area).

RQD correlates with *UCS* and a regression relationship is provided. To the authors' knowledge, there is no relationship between *RQD* and *UCS* for limestone in the literature. So, the proposed mathematical relationship can be considered as a useful equation that links two key parameters, the *RQD* provided from borehole drilling as a field test and *UCS* provided from unconfined compression as a laboratory test. Figure 2 shows the trends of E_m/UCS with *RQD* and 1-*RQD*. The two representations are often used by engineers depending on the application (for example, see [3]).

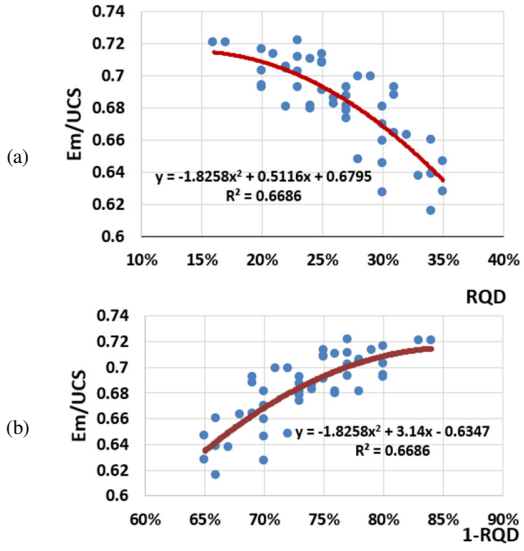

Fig. 2. (a) E_m/UCS against RQD, (b) E_m/UCS against (1- RQD).

IV. GEOPHYSICAL INVESTIGATION USING GPR

GPR tests were performed on the site to detect karstic cavities. The principle of this method is to follow the shape of the EM waves, where their propagation and reflection depend on the contrast of the electric properties of the medium. Hyperbolic curves in GPR data serve as representations of target shapes [22-24]. The targets must exhibit contrasting electric properties, with the dielectric constant and electrical conductivity being directly proportional to the magnitude of this contrast [24]. Figure 3 shows the procedure followed to obtain the GPR data, and some corresponding GPR results are summarized in Figure 4. See [24] for more details on the reflections from voids (or cavities) and the reverse polarity on the radargram reflections.

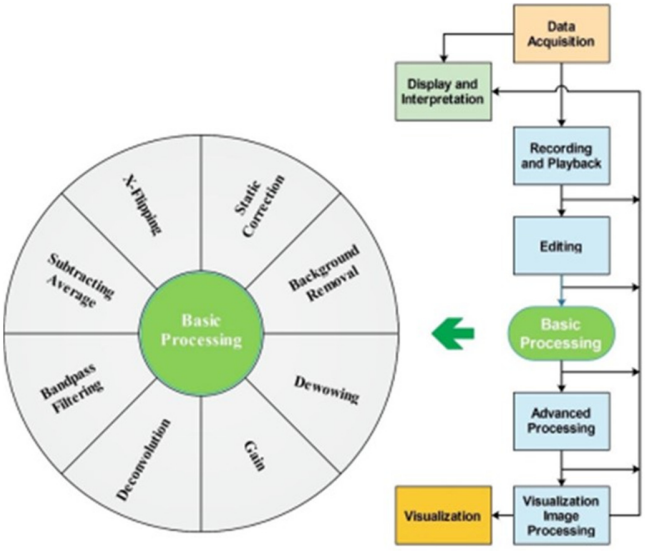

Fig. 3. A general overview of GPR data processing flow.

Figure 4 shows two examples of 2D radargrams (2D distributions of reflected waves), providing clear identification of the cavities locations for each profile. Areas of weakness corresponding to cavities are delineated by circles where the hyperboles appeared in restricted areas. These cavities are approximated in terms of shape and depth and distinctly marked by circles. The hyperbolic shape of the EM direction depicts the location of the cavity. Figure 4 emphasizes the presence of high-amplitude reflections, indicating the presence of cavities at a depth of 1.5 and 2.5 m. Other radargrams showed reflections that occurred at a depth exceeding 3.5 m.

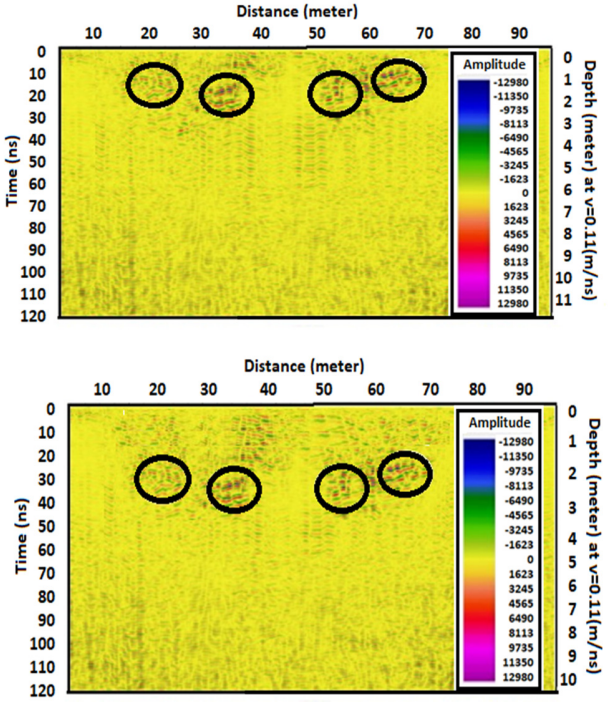

Fig. 4. 2D radargrams: circles delineate weak zones and karstic cavities.

V. MODIFIED GENERALIZED HOEK-BROWN CRITERION OF WEAK LIMESTONE ROCK DEPOSIT CONTAINING KARSTIC CAVITIES

The basic Hoek-Brown criterion is a well-known criterion for rocks, with its most recent update (2002 edition). Recently, a few changes were proposed in the empirical parameters introduced in the mathematical relationships by considering the dependence of the GSI on discontinuities such as joints. In the Hoek-Brown criterion, the strength and deformation properties of intact rock, derived from laboratory tests, are reduced based on the properties of discontinuities in the rock mass. In the limestone rock studied here, to consider the influence of crushing and the presence of cavities (voids assumed as huge discontinuities), correlations between *GSI* and *RQD* were proposed, and then between *GSI*, *RQD*, and the amplitude reflections A_i of the EM wave to assure the applicability of the criterion to very weak rock masses with cavities (karstic cavities as a specific case). The main proposed changes in the generalized Hoek-Brown criterion are as follows. Equation (4) is the standard form of the Hoek-Brown criterion. Equations (5), (6), and (7) give the relationships between the parameters of the model and *GSI*. Finally, (8) provides a new definition of *GSI* as a function of *RQD* and the dimensionless amplitude A_i/A_0 of the EM wave.

$$\sigma_1 = \sigma_3 + \sigma_{ci}\ (m_b \frac{\sigma_3}{\sigma_{ci}} + s)^{\alpha} \quad (4)$$

$$m_b = \sigma_3 + m_b\ exp[(GSI - 100)\,(28 - 14\,D)\,] \quad (5)$$

$$s = exp[(GSI - 100)\,/(9 - 3\,D)\,] \quad (6)$$

$$a = 0.5 + \frac{1}{6}\,[exp(-GSI/15)\ - exp(-20/3)\,] \quad (7)$$

$$GSI = g\left[RQD, \frac{Ai'}{A0}\right] \quad (8)$$

where A_i is the amplitude of the reflected wave at the cavity location and A_0 is the amplitude reference. As can be observed, contrary to the initial case where GSI was initially introduced as a geologic parameter estimated qualitatively from geological observations in the field, in the proposed new formulation, *GSI* is linked directly to *RQD* and the amplitude reflection A_i of the EM wave, including in such way the data from GPR of the karstic cavity, and g is a given function. Furthermore, D is a disturbance factor that depends on the degree of disturbance of the rock mass and varies from 0 for undisturbed in situ rock masses to 1 for very disturbed rock masses. In (8), a is a material parameter.

Consider the results given in [15], given three functions for respectively $D = 0$, $D = 0.5$, and $D = 1$ that link E_{rm}/UCS with *GSI*. Figure 5 presents only the case of $D = 1$ for a high-weathered rock. The mathematical relationships for three values of D are given based on the fitting of data presented in [15]. Considering the highly weathered and crushable character of limestone, D is fixed to 1. Then, *GSI* is obtained as a function of *RQD*. Figure 6 shows the *GSI* against *RQD*, obtained based on the following process or algorithm.

$$\frac{E_{rm}}{UCS} = f_1(GSI)\ from\ [\ \ ] \rightarrow GSI = f^{-1}\left(\frac{E_{rm}}{UCS}\right)$$

Then, using experimental results in Table II provides:

$$GSI = f^{-1}\left(\frac{E_{rm}}{UCS}\right)$$

where E_{rm}/UCS data are given in Table II.

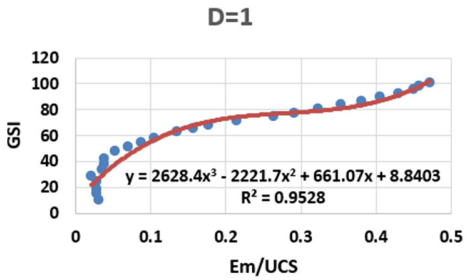

Fig. 5. GSI against E_m/UCS (data from [15]).

Figure 6 shows the *GSI* against *RQD* considering an average value of A_i/A_0. This curve is deduced using the fitting equation between *GSI* and both *UCS* and rock mass modulus:

$$GSI = 2628.4\left(\frac{E_m}{UCS}\right)^3 - 2221.7\left(\frac{E_m}{UCS}\right)^2 + 661.07\left(\frac{E_m}{UCS}\right) + +8.84 \quad (9)$$

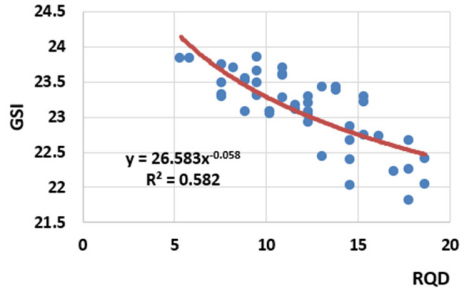

Fig. 6. GSI against (E_m/UCS) for the weak and crushable limestone.

In the case of karstic cavities, for which GPR data are available and the instantaneous amplitude A_i is obtained, *GSI* can be defined explicitly and (8) becomes:

$$GSI = g\left[RQD, \frac{Ai'}{A0}\right] = \frac{Ai}{A0}\, g[RQD] \quad (10)$$

where g is given by the equation in Figure 6.

VI. CONCLUSION

The findings of this study pertain to a site with a limestone rock deposit with underground karstic cavities. Unconfined compressive tests were performed and conducted to determine the *UCS* values and the rock mass modulus. *RQD* was determined from the boreholes and drilling for a field area of 473480 m^2. The correlation between E_m/UCS and *RQD* was provided and analyzed. Based on the new interpretation of the *GSI* relationship with the rate E_m/UCS, a mathematical relationship was given to link *GSI* and *RQD*. By mitigating the issue of random cavity distribution through in-depth interpretation of cross-GPR sections, qualitative instantaneous amplitude reflected EM waves were introduced in the mathematical relationship between *GSI* and *RQD*. *GSI* decreases with increasing instantaneous amplitude, which indicates existing karstic cavities. The generalized Hoek-Brown criterion was modified by involving both RQD quantitative data from drilling log data and the amplitude of reflected EM waves provided by radar ground penetration field tests. The results presented shed light on a potential correlation between E_m/UCS and *RQD* and then between *GSI* and *RQD*, using a function linking E_m/UCS and *RQD*. This suggests that geotechnical investigations may precede complementary GPR surveys as successive steps. Thus, the correlation between *GSI* and *RQD* was extended by introducing the quantitative data provided by GPR (instantaneous amplitude of the reflected EM wave). The future scope of this research is to collect more relevant geophysical data, particularly GPR information on cavities, stochastic field data, and basic laboratory results commonly used in the rock mechanics framework. Such findings can be used to build some practical charts for a better engineering system for classifying weak rocks, providing a quick estimate of the engineering properties of weathered karstic rocks.

ACKNOWLEDGMENT

The authors acknowledge the approval and support of this research study by grant no. ENGA-2022-11-1572 from the Deanship of Scientific Research, Northern Border University, Arar, KSA.

REFERENCES

[1] Y. Koobaa, H. Guiras, and M. Jamei, "Compression and shear strengths of sandy limestone and the role of the porosity: a case study," *Soils and Rocks*, vol. 43, no. 4, pp. 693–705, Oct. 2020, https://doi.org/10.28927/SR.434693.

[2] H. Daoud, K. Rashed, and Y. Alshkane, "Correlations of Uniaxial Compressive Strength and Modulus of Elasticity with Point Load Strength Index, Pulse Velocity and Dry Density of Limestone and Sandstone Rocks in Sulaimani Governorate, Kurdistan Region, Iraq.," *Journal of Zankoy Sulaimani - Part A*, vol. 19, no. 3–4, pp. 57–72, 2017, https://doi.org/10.17656/jzs.10632.

[3] S. Vidana Pathiranagei, I. Gratchev, C. Cui, and B. Elsmore, "New weathering classification system of rocks based on the engineering properties," *Bulletin of Engineering Geology and the Environment*, vol. 82, no. 2, Feb. 2023, Art. no. 60, https://doi.org/10.1007/s10064-023-03071-0.

[4] S. M. Shaaban and S. Z. Tawfik, "Classification of Volcanic Rocks based on Rough Set Theory," *Engineering, Technology & Applied Science Research*, vol. 10, no. 2, pp. 5501–5504, Apr. 2020, https://doi.org/10.48084/etasr.3420.

[5] G. R. Lashkaripour, "Predicting mechanical properties of mudrock from index parameters," *Bulletin of Engineering Geology and the Environment*, vol. 61, no. 1, pp. 73–77, Feb. 2002, https://doi.org/10.1007/s100640100116.

[6] M. H. Leite and F. Ferland, "Determination of unconfined compressive strength and Young's modulus of porous materials by indentation tests," *Engineering Geology*, vol. 59, no. 3, pp. 267–280, Apr. 2001, https://doi.org/10.1016/S0013-7952(00)00081-8.

[7] G. M. Elliott and E. T. Brown, "Yield of a soft, high porosity rock," *Géotechnique*, vol. 35, no. 4, pp. 413–423, Dec. 1985, https://doi.org/10.1680/geot.1985.35.4.413.

[8] E. Hoek and M. S. Diederichs, "Empirical estimation of rock mass modulus," *International Journal of Rock Mechanics and Mining Sciences*, vol. 43, no. 2, pp. 203–215, Feb. 2006, https://doi.org/10.1016/j.ijrmms.2005.06.005.

[9] Z. Li, Y. Xiao, R. Pigrim, J. Royce, and S. Butt, "Subsurface rock interface imaging with the application of Ground Penetrating Radar (GPR)," presented at the 72nd Canadian Geotechnical Society Annual Conference, St. John's, Canada, Sep. 2019.

[10] A. A. Cigna, "A classification of karstic phenomena," *International Journal of Speleology*, vol. 10, no. 1, pp. 3–9, 1978.

[11] Ó. P. Anchuela, A. M. Casas-Sainz, A. Pocoví-Juan, H. G. Garbí, and P. Calvín, "Characterization of the Karstic Process in an Urban Environment Using GPR Surveys," *Journal of Materials in Civil Engineering*, vol. 26, no. 8, Aug. 2014, Art. no. 05014004, https://doi.org/10.1061/(ASCE)MT.1943-5533.0001072.

[12] A. T. Chamberlain, W. Sellers, C. Proctor, and R. Coard, "Cave Detection in Limestone using Ground Penetrating Radar," *Journal of Archaeological Science*, vol. 27, no. 10, pp. 957–964, Oct. 2000, https://doi.org/10.1006/jasc.1999.0525.

[13] E. T. Brown, "Strength of Models of Rock with Intermittent Joints," *Journal of the Soil Mechanics and Foundations Division*, vol. 96, no. 6, pp. 1935–1949, Nov. 1970, https://doi.org/10.1061/JSFEAQ.0001479.

[14] J. Zuo, H. Liu, and H. Li, "A theoretical derivation of the Hoek–Brown failure criterion for rock materials," *Journal of Rock Mechanics and Geotechnical Engineering*, vol. 7, no. 4, pp. 361–366, Aug. 2015, https://doi.org/10.1016/j.jrmge.2015.03.008.

[15] E. Hoek and E. T. Brown, "The Hoek–Brown failure criterion and GSI – 2018 edition," *Journal of Rock Mechanics and Geotechnical Engineering*, vol. 11, no. 3, pp. 445–463, Jun. 2019, https://doi.org/10.1016/j.jrmge.2018.08.001.

[16] H. Gasmi, M. Touahmia, A. Torchani, E. Hamdi, and A. Boudjemline, "Determination of Fractured Rock's Representative Elementary Volume by a Numerical Simulation Method," *Engineering, Technology & Applied Science Research*, vol. 9, no. 4, pp. 4448–4451, Aug. 2019, https://doi.org/10.48084/etasr.2854.

[17] E. Hoek, "Fracture of anisotropic rock," *Journal of the South African Institute of Mining and Metallurgy*, vol. 64, no. 10, pp. 501–518, May 1964.

[18] E. Hoek and C. D. Martin, "Fracture initiation and propagation in intact rock – A review," *Journal of Rock Mechanics and Geotechnical Engineering*, vol. 6, no. 4, pp. 287–300, Aug. 2014, https://doi.org/10.1016/j.jrmge.2014.06.001.

[19] N. Vlachopoulos, M. S. Diederichs, V. Marinos, and P. Marinos, "Tunnel behaviour associated with the weak Alpine rock masses of the Driskos Twin Tunnel system, Egnatia Odos Highway," *Canadian Geotechnical Journal*, vol. 50, no. 1, pp. 91–120, Jan. 2013, https://doi.org/10.1139/cgj-2012-0025.

[20] O. Rincon, A. Shakoor, and M. Ocampo, "Investigating the reliability of H/V spectral ratio and image entropy for quantifying the degree of disintegration of weak rocks," *Engineering Geology*, vol. 207, pp. 115–128, Jun. 2016, https://doi.org/10.1016/j.enggeo.2016.04.020.

[21] O. Rincón and M. Ocampo, "Weak rocks disintegration patterns recognition through image analysis," in *2017 Fifteenth IAPR International Conference on Machine Vision Applications (MVA)*, Nagoya, Japan, May 2017, pp. 338–341, https://doi.org/10.23919/MVA.2017.7986870.

[22] S. Birkenfeld, "Automatic detection of reflexion hyperbolas in gpr data with neural networks," in *2010 World Automation Congress*, Kobe, Japan, Sep. 2010, pp. 1–6.

[23] L. Mertens, R. Persico, L. Matera, and S. Lambot, "Automated Detection of Reflection Hyperbolas in Complex GPR Images With No A Priori Knowledge on the Medium," *IEEE Transactions on Geoscience and Remote Sensing*, vol. 54, no. 1, pp. 580–596, Jan. 2016, https://doi.org/10.1109/TGRS.2015.2462727.

[24] M. Robinson, C. Bristow, J. McKinley, and A. Ruffell, "1.5.5. Ground Penetrating Radar," *Geomorphological Techniques*, 2013.